

University of Rhode Island

DigitalCommons@URI

---

Physical Oceanography Technical Reports

Physical Oceanography

---

2016

## Sub-Antarctic Flux and Dynamics Experiment Inverted Echo Sounder Data Report for March 1995 to March 1997

Karen L. Tracey

*Graduate School of Oceanography, University of Rhode Island*

D. Randolph Watts

*Graduate School of Oceanography, University of Rhode Island*

Follow this and additional works at: [https://digitalcommons.uri.edu/physical\\_oceanography\\_techrpts](https://digitalcommons.uri.edu/physical_oceanography_techrpts)

---

### Recommended Citation

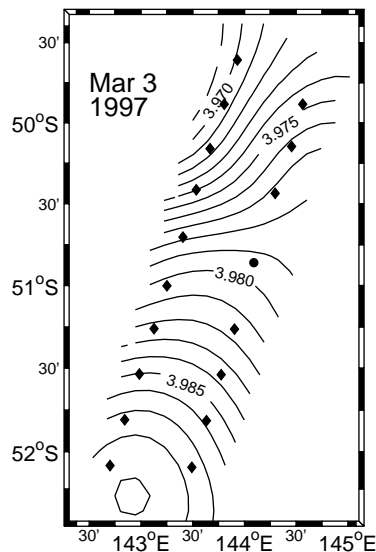
Tracey, Karen L. and Watts, D. Randolph, "Sub-Antarctic Flux and Dynamics Experiment Inverted Echo Sounder Data Report for March 1995 to March 1997" (2016). *Physical Oceanography Technical Reports*. Paper 5.

[https://digitalcommons.uri.edu/physical\\_oceanography\\_techrpts/5](https://digitalcommons.uri.edu/physical_oceanography_techrpts/5)

This Article is brought to you for free and open access by the Physical Oceanography at DigitalCommons@URI. It has been accepted for inclusion in Physical Oceanography Technical Reports by an authorized administrator of DigitalCommons@URI. For more information, please contact [digitalcommons-group@uri.edu](mailto:digitalcommons-group@uri.edu).

GRADUATE SCHOOL OF OCEANOGRAPHY  
UNIVERSITY OF RHODE ISLAND  
NARRAGANSETT, RHODE ISLAND

**Sub-Antarctic Flux and Dynamics Experiment  
Inverted Echo Sounder Data Report  
for March 1995 to March 1997**



**Karen L. Tracey  
and  
D. Randolph Watts**

In house document January 2001

Published online January 2016

[http://digitalcommons.uri.edu/physical\\_oceanography\\_techrpts/5/](http://digitalcommons.uri.edu/physical_oceanography_techrpts/5/)

*This research program has been sponsored by the National Science Foundation under grants  
OCE9204041 and OCE9912320*



# Contents

<b>List of Tables</b>	<b>ii</b>
<b>List of Figures</b>	<b>ii</b>
<b>1 Introduction</b>	<b>1</b>
<b>2 Inverted Echo Sounder Description</b>	<b>4</b>
<b>3 Data Processing</b>	<b>4</b>
3.1 Time Base . . . . .	4
3.2 Travel Time Processing . . . . .	5
3.2.1 Instrument Depth . . . . .	5
3.2.2 Seasonal Correction . . . . .	6
3.2.3 Conversion to Dynamic Travel Time . . . . .	6
3.2.4 Calibration to $\tau_{3000}$ . . . . .	7
<b>Acknowledgments</b>	<b>10</b>
<b>References</b>	<b>11</b>

## List of Tables

1	Site Locations . . . . .	3
---	--------------------------	---

## List of Figures

1	Moored Instrument Sites . . . . .	2
2	$\tau_{3000}$ versus $\tau_{2000}$ and $\tau_{4000}$ . . . . .	8
3	Conversion coefficients for $\tau_{3000}$ . . . . .	9



# 1 Introduction

This report focuses on the inverted echo sounder (IES) data collected as part of the Sub-Antarctic Flux and Dynamics Experiment (SAFDE) during March 1995 – March 1997. The collection, processing and calibration of the IES data are described herein. The measurements were made under the support of the National Science Foundation. Other instruments moored as part of the experiment included horizontal electric field recorders (HEF) and current meter moorings (CM). The HEF and CM data sets are not documented in this report.

The moored instrument locations are shown in Figure 1. The IES sites were spaced about 30 km apart along two lines spanning the Subantarctic Front (SAF). The two lines were separated zonally by approximately 50 km, and their orientation was chosen to be perpendicular to the mean path of the SAF. The IESs were positioned so that groups of three sites formed triangles within which the two-dimensional horizontal gradients of geopotential could be estimated from the measurements.

Table 1 summarizes the deployment locations of the IESs. The instruments were deployed on a cruise aboard the R/V Melville (ML9511) during March 18 – April 14, 1995. The instruments were recovered during March 8 – April 5, 1997 aboard the R/V Meville (ML9706).

All IESs were successfully recovered, although several difficulties were encountered with IES 16. Initially, the instrument would not accept the release command. We noticed that a second return accompanied every beacon ping which we determined was an echo off a nearby cliff. IES 16 finally accepted the release command after the ship was repositioned to avoid the bottom interference. Subsequently, IES 16 did not leave the bottom in the usual amount of time. We left the site to do other work and returned about 22 hours later. The IES was no longer on the bottom. The instrument had drifted about 8 nm from the site. Subsequent data processing revealed that the IES had left the bottom 10 hours after the release command was issued. We found tiny mussel-like creatures on the instrument, so it is possible that they interfered with the release mechanism.

Two of the instruments suffered partial data losses. IES 4 had severe tape recorder problems which resulted in substantial data loss. Only the initial 130 days of data, which had better quality, have been retained. The travel time data of IES 12 were exceptionally noisy during an 155-day period in the austral winter/spring 1995. After processing the record through the standard steps, it

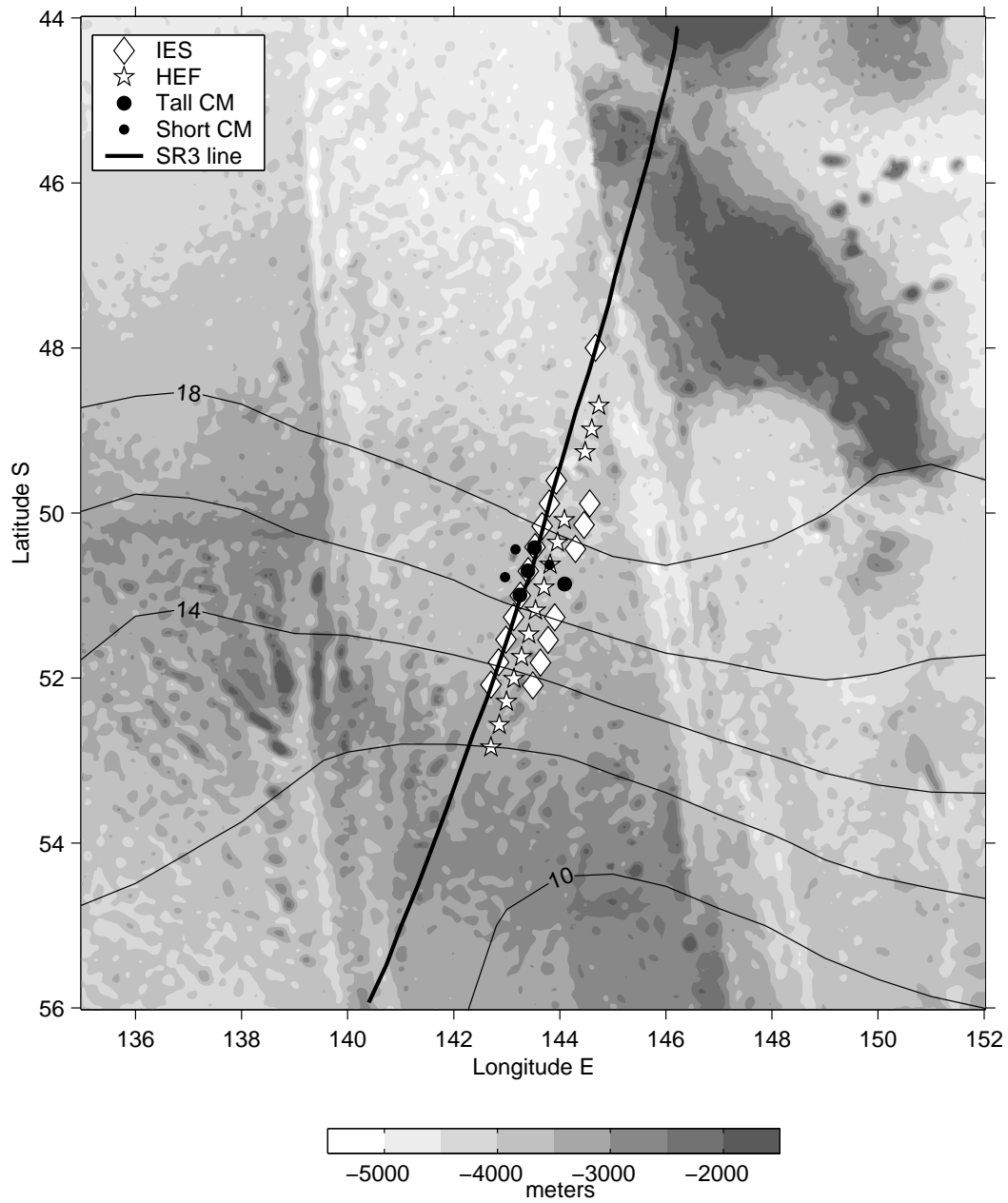


Figure 1: Locations of 18 IESs (diamonds), 14 HEFs (stars), and 7 CMs (large and small circles) deployed across the Subantarctic Front. Only recovered instruments are shown. The solid bold line indicated the WOCE SR3 hydrographic line. Geopotential height ( $\text{m}^2 \text{s}^{-1}$ ) is contoured to show the mean SAF baroclinic structure ( $\phi_{0-2000}$  calculated from the gridded data set of Olbers et al. [1992]). The colorbar indicates the shading of the bottom topography.



Table 1: **SAFDE IES Location Information**

Site	Latitude(S)	Longitude(E)	Transducer Size
IES 1	47°59.92'	144°40.40'	Big
IES 2	49°36.50'	143°56.00'	Big
IES 3	49°53.05'	144°33.85'	Small
IES 4	49°53.05'	143°48.30'	Small
IES 5	50°08.75'	144°27.35'	Big
IES 6	50°09.62'	143°40.12'	Big
IES 7	50°26.15'	144°17.80'	Small
IES 8	50°24.85'	143°32.15'	Small
IES 9	50°42.27'	143°24.38'	Small
IES 10	51°00.05'	143°15.15'	Big
IES 11	51°15.85'	143°54.25'	Small
IES 12	51°15.70'	143°07.65'	Small
IES 13	51°32.30'	143°46.60'	Small
IES 14	51°32.10'	142°59.20'	Big
IES 15	51°48.85'	143°38.00'	Big
IES 16	51°48.50'	142°50.65'	Big
IES 17	52°05.47'	143°29.55'	Big
IES 18	52°04.88'	142°42.10'	Big

was determined that the character of the record during that time period was distinct from all other IES records. Thus, the data during that time period have been excluded.

## 2 Inverted Echo Sounder Description

The inverted echo sounders used in the SAFDE experiment were built at URI. Chaplin and Watts [1984] provide a description of the IES circuitry and mooring configuration.

The instruments were moored one meter above the ocean floor and sampled at hourly intervals throughout the deployment period. At the designated sampling time, a burst of 24 acoustic pulses (10 KHz) were transmitted at 10 second intervals, and the time each ping took to travel the round trip distance to the sea surface was measured and recorded on the internal cassette tape.

For typical deployment depths of 3000–5000 m, the full travel times ( $\tau$ ) range between 4–7 s; thus with a resolution of 0.05 ms, each measurement would require a storage space of 18 bits on the cassette tape. However since the variability of the travel time signal in major current regions such as the Subantarctic Front is only 0.03–0.06 s, it is not necessary to record the full  $\tau$  measurement. By recording just the 13 least significant bits, variability of up to 0.4 s can be resolved, with only a constant integer multiple of 0.4 s excluded. The constant can be determined a priori by knowing the bottom depth at the instrument site to within 300 m; it may be added back into the recorded travel times after the instrument is recovered. The advantage of recording only the variable part of the  $\tau$  measurements is that space is conserved on the cassette tape, allowing the length of deployment to be extended. The appropriate constant has been added to each hourly record.

## 3 Data Processing

### 3.1 Time Base

Timing of each sample period is referenced to the transmission time of the first travel time ping in the sample burst as it is easily observed. The midpoint of the burst of 24 measurements is located at 115 s, since the pings were sent at 10 s intervals. The date and time were assigned to the midpoint of each sampling period and these are listed in the data files.

## 3.2 Travel Time Processing

The basic steps in the IES data processing included transcription from the cassette tape, editing to remove data spikes, and conversion of the recorded counts into round trip travel times ( $\tau$ ). From the 24 travel times taken during each sampling period a single representative  $\tau$  was chosen by seeking the first quartile value of a windowed Rayleigh distribution [Watts and Rossby, 1977; Fields *et al.*, 1991]. After removing data spikes, the hourly  $\tau$  records were low-pass filtered using a fourth-order Butterworth filter with a cutoff period of 72 hours. The filter was passed forward and backward in time to avoid introducing phase shifts. Twenty hours of data at each end of the filtered series were discarded to avoid startup transients. After filtering, the timeseries were subsampled at daily intervals centered at 1200 UT. Subsequently, the travel times were adjusted by the series of processing steps described next to project them on to a common pressure level. The initial data processing was accomplished by a set of MATLAB [The MathWorks, Inc., 1992] routines adapted from previously-developed FORTRAN routines [Fields *et al.*, 1991]. Projection on to the common pressure level was done using a set of MATLAB codes written by C. Sun.

### 3.2.1 Instrument Depth

The bottom depth at each IES site was measured on board ship during the deployment cruise. While the accuracy of this measurement is adequate for determining the unrecorded travel time constant ( $\tau_c$ ) it is insufficient for projecting onto a common pressure level. A more accurate pressure depth estimate was obtained by using hydrographic casts to calculate and integrate sound speed profiles

$$\tau = 2 \int_0^{P_B} \frac{dp}{\rho g c} \quad (1)$$

where gravity  $g$  depends on the latitude and  $P_B$  is the deep pressure limit of integration. A hydrocast was used for these calculations if its position was within 3 km of an IES site if it occurred no more than 31 hours prior to the instrument deployment or after the recovery. The sound speed profile between the sea surface and a preliminary IES pressure estimate was calculated for each cast. Because CTD casts, even going near the bottom, do not typically quite reach the pressure of the IES on the bottom, we linearly extrapolated the sound speed profile to the preliminary IES

pressure. The mean sound speed ( $\overline{1/\rho g c}$ ) was then combined with the concurrently measured  $\tau$  by the IES (a 3-hour mean value, including  $\tau_c$ , excluding a 0.003 s internal detection delay, and divided by two) to determine an accurate pressure for the IES. The final pressure ( $P_{\text{IES}}$ ) of each IES was calculated as the average of the estimates obtained by this procedure for all hydrocasts (usually 2–4) at that site. The rms uncertainty of  $P_{\text{IES}}$  ranged from a low of 0.07 dbar for IES 6 to a high of 1.97 dbar for IES 11. The overall mean rms uncertainty  $P_{\text{IES}}$  for the 18 IESs was  $0.63 \pm 0.42$  dbar. The largest uncertainties were obtained at four sites which had small transducers as well as at IES 4 which had tape problems. Excluding these five records reduces the mean rms uncertainty to  $0.45 \pm 0.21$  dbar for the remaining 13 records.

### 3.2.2 Seasonal Correction

Watts *et al.* [2001] determined the annual cycle of acoustic travel time through the upper 300 dbar. The signal varied by less than 0.8 ms, with the maximum occurring in August and the minimum in March. “De-seasoned”  $\tau$  were calculated by subtracting the annual cycle shown in their Figure A1b from the lowpass filtered values.

### 3.2.3 Conversion to Dynamic Travel Time

The IES  $\tau$  measurements are used together with GEM fields [Watts *et al.*, 2001] to determine the vertical structure of temperature, salinity, and specific volume anomaly in the overlying water column. These two-dimensional GEM fields were generated from hydrographic data as functions of pressure and travel time, where  $\tau$  was integrated between constant pressure limits instead of metric depths. Travel time calculated in this manner becomes a function of density ( $\rho$ ) and gravity ( $g$ ) as well as sound speed ( $c$ ). Because gravity changes with latitude (from  $9.78 \text{ m s}^{-2}$  at the equator to  $9.83 \text{ m s}^{-2}$  at the pole), the travel time associated with a water column of constant 3000 dbar would differ by 0.8 ms for the 2-degree latitude change across the SAFDE array. This difference is the same magnitude as the seasonal variation just discussed.

A simple solution is to calculate ‘dynamic travel time’ ( $\tau^*$ ) independent of latitude by specifying gravity (in Equation 1) as a constant. We used  $g = g_o = 9.8 \text{ m s}^{-2}$ . GEM fields parameterized by  $\tau^*$  are also independent of latitude. This procedure offers the same advantage to  $\tau$  calculations

as ‘dynamic height’ offers to height  $z$  calculations (which otherwise would depend on  $g$ ).

The IES  $\tau$  measurements must be converted to  $\tau^*$  in order to interpret them with the GEM fields. A good empirical relation is

$$\tau^* = \frac{g(\lambda_{\text{IES}}, 0)}{g_o(1 - \frac{P_{\text{IES}}}{1.015R})} \tau_{\text{IES}}$$

where the earth’s radius  $R = 6.371 \times 10^6$  m,  $P_{\text{IES}}$  is the pressure of the IES (with  $P_{\text{IES}}/1.015$  a representation of the IES depth adequate for these purposes), and  $g(\lambda_{\text{IES}}, 0)$  is gravity at the sea surface at the latitude of the IES site.

### 3.2.4 Calibration to $\tau_{3000}$

The IES-measured  $\tau$ s depend on the bottom depth as well as on the water properties above the instrument. However, bottom depths vary from site to site and never exactly coincide with the 3000 dbar integration limit used for the GEM field parameterizations. Thus, the measured travel times must be projected onto the 3000 dbar pressure level.

The projections were empirically derived using the hydrographic data collected along the WOCE SR3 line by S. Rintoul and during the SAFDE launch and recovery cruises. Each hydrocast was integrated from a suite of pressure levels ( $p$ ) to the surface to simulate dynamic travel time ( $\tau_p^*$ ). For this study,  $\tau_p^*$  was simulated for  $p = 2000$ – $4500$  dbar at 50 dbar intervals. Figure 2 shows examples of the relationships for travel times at 3000 dbar ( $\tau_{3000}^*$ ) versus  $\tau_p^*$  obtained for pressures of 2000 and 4000 dbar.

Second order polynomials were fitted to these relationships. However because the variations in  $\tau_p^*$  were on the order of tens of milliseconds while the magnitudes were on the order of several seconds, large errors could have arisen when determining the coefficients. To minimize the errors, the coefficients were obtained using only the  $\tau_p^*$  variability, determined by removing a large constant from the travel times. This constant,  $\tau_{\text{so}}(p)$ , was defined as the round trip travel time that would be measured if the sound speed in the ocean was fixed at  $1500 \text{ m s}^{-1}$ :

$$\tau_{\text{so}}(p) = \frac{2p}{1500}$$

The coefficients of the second-order polynomials differed for each pressure level as shown in Figure 3.

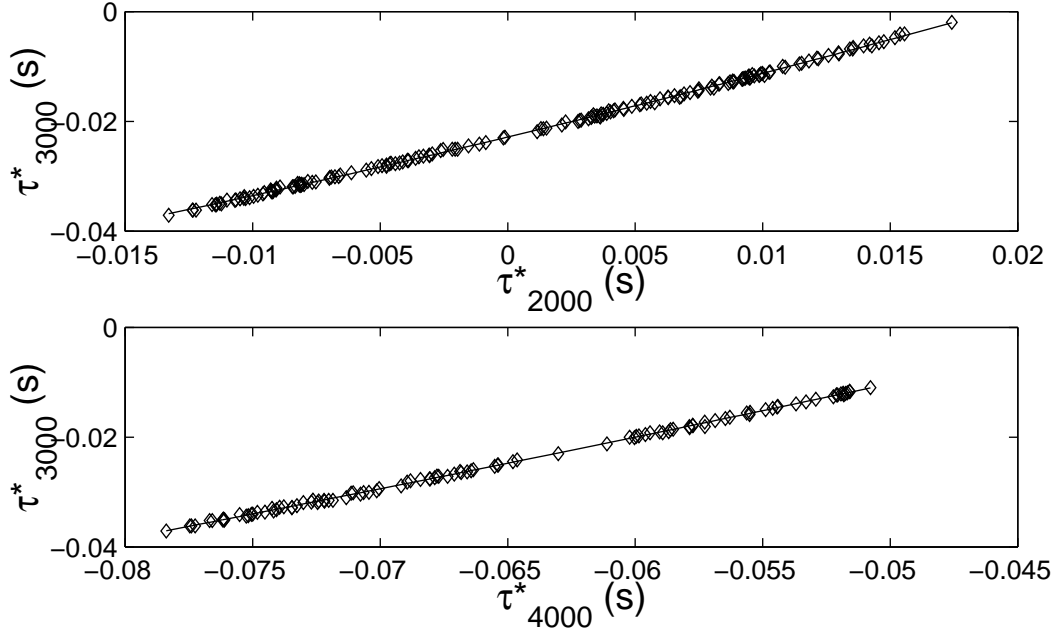


Figure 2: Comparison of the round trip travel time for a bottom pressure of 3000 dbar with the travel times for bottom pressures of 2000 dbar (top) and 4000 dbar (bottom).

Finally, the travel times measured by each IES were projected onto the 3000 dbar level as

$$\tau_{3000} = \mathbf{A}(p)\tau'^2 + \mathbf{B}(p)\tau' + \mathbf{C}(p) + \tau_{\text{so}}(3000)$$

where  $\tau' = \tau_p^* - \tau_{\text{so}}(p)$  and  $p = P_{\text{IES}}$ .

Contributing to the uncertainty in  $\tau_{3000}$  are the accuracy of the travel time measurements,  $\epsilon_{\tau} = 1.0$  ms [Chaplin and Watts, 1984], and the accuracy of the bottom pressure of about 0.5 dbar which is equivalent to a  $\epsilon_p = 0.7$  ms error in travel time. Additional error in  $\tau_{3000}$  arises from the projection to 3000 dbar from the actual bottom pressure. These errors  $\epsilon_{\text{proj}}$  are estimated to be 0.2 ms. Thus the total error in  $\tau_{3000}$  is estimated as  $(\epsilon_{\tau}^2 + \epsilon_p^2 + \epsilon_{\text{proj}}^2)^{\frac{1}{2}} = 1.2$  ms.

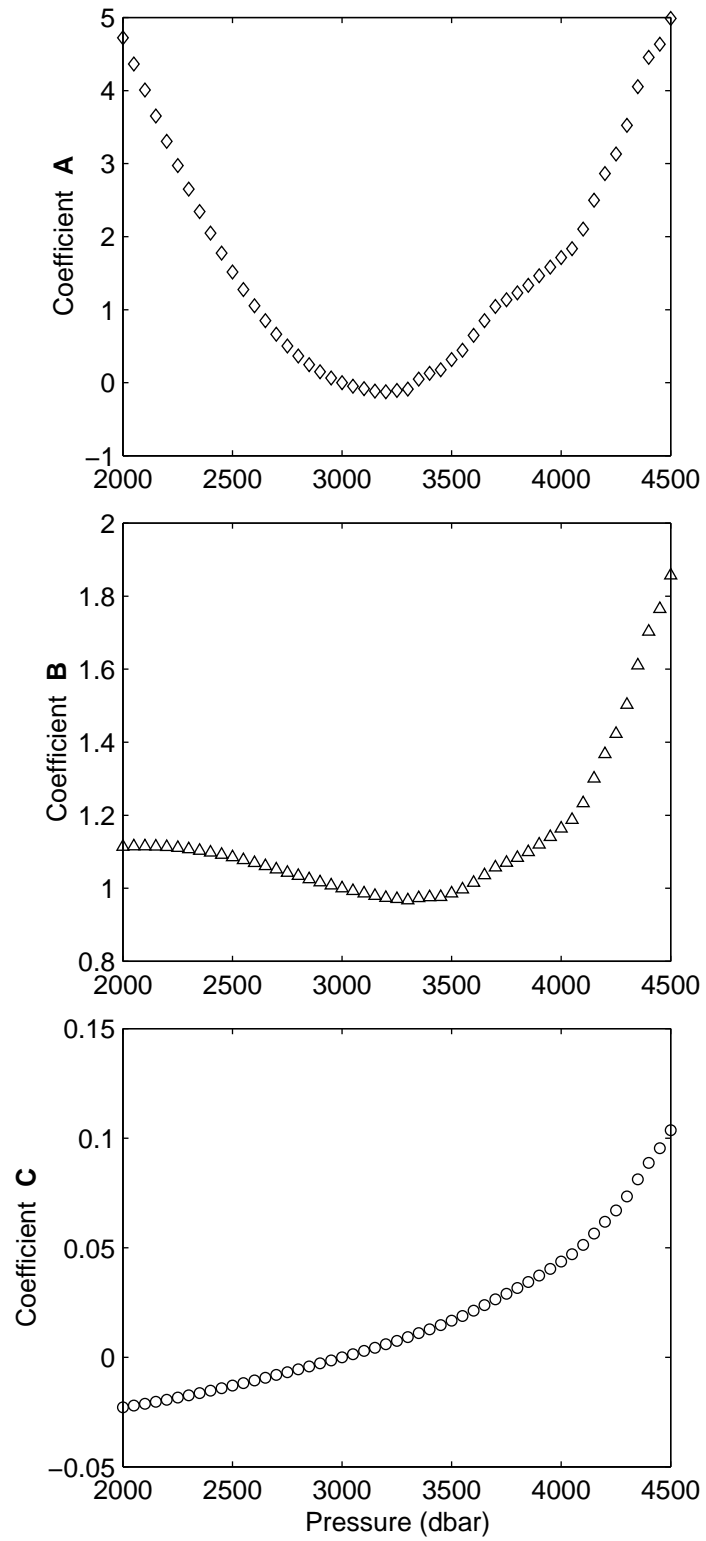


Figure 3: Coefficients A, B, and C, plotted as functions of bottom pressure, are used to convert  $\tau_p^*$  to  $\tau_{3000}$

### **Acknowledgments**

This experiment was supported by the National Science Foundation under grants OCE9204041 and OCE9912320. We thank the crew of the R/V Melville for their efforts during the deployment and recovery cruises. The inverted echo sounder preparation was performed by Michael Mulroney. Che Sun projected the travel time records onto the common pressure level.



## REFERENCES

- Chaplin, G. and D. R. Watts. 1984. Inverted echo sounder development. *Oceans '84 Conference Record. 1*. 249–253.
- Fields E., K.L. Tracey, and D. R. Watts. 1991. Inverted echo sounder processing procedures. University of Rhode Island. GSO Technical Report 91–3. 180 pp.
- The MathWorks, Inc. 1992. *MATLAB Reference Guide*. Natick, MA.
- Olbers, D., V. Gouretski, G. Seiß, and J. Schröter. 1992. *Hydrographic atlas of the Southern Ocean*. Alfred Wegner Institute, Bremerhaven, Germany.
- Tracey, K. L., S. D. Howden, and D. R. Watts. 1997. IES calibration and mapping procedures. *J. Atmos. Oceanic Technol.*, 14, 1483–1493.
- Watts, D. R. and H.T. Rossby. 1977. Measuring dynamic heights with inverted echo sounders: Results from MODE. *J. Phys. Oceanogr.*, 7, 345–358.
- Watts, D. R., C. Sun, and S. Rintoul. 2001. A two-dimensional gravest empirical mode determined from hydrographic observations in the Subantarctic Front. *J. Phys. Oceanogr.*, 31, 2186–2209.